Waveform-Dependent Influence of Electrical Vestibular Stimulation on EEG Revealed by Granger Causality

Maryam Kia
Canadian Centre for Behavioural Neuroscience
University of Lethbridge
Lethbridge, Canada
m.kiakojouri@uleth.ca

Sepideh Hajipour Sardouie
Pacific Parkinson Research Centre
University of British Columbia
Vancouver, Canada
sepideh.hajipour@ubc.ca

Maryam S. Mirian
Pacific Parkinson Research Centre
University of British Columbia
Vancouver, Canada
maryam.mirian@ubc.ca

Matthew Tata
Canadian Centre for Behavioural Neuroscience
University of Lethbridge
Lethbridge, Canada
matthew.tata@uleth.ca

Artur Luczak
Canadian Centre for Behavioural Neuroscience
University of Lethbridge
Lethbridge, Canada
Luczak@uleth.ca

Martin J McKeown
Pacific Parkinson Research Centre
Faculty of Medicine
University of British Columbia
Vancouver, Canada
martin.mckeown@ubc.ca

***Abstract*—Electrical Vestibular Stimulation (EVS) is a non-invasive neuromodulation technique with reported benefits for motor and balance function in Parkinson's disease (PD); however, a principled understanding of how stimulation waveform characteristics influence neural activity remains limited. Here, we systematically characterized waveform-dependent neural responses to EVS using a stimulus–response framework based on Granger Causality (GC) applied to electroencephalography (EEG). EEG was recorded from healthy controls and individuals with PD during exposure to a large set of 304 distinct EVS waveforms. GC was used to quantify the directed influence of each stimulation waveform on independent EEG components. Each EVS waveform was represented by a GC-based response pattern across components, and waveforms were clustered based on similarities in these patterns to identify distinct classes of neural responses. This analysis revealed a highly structured response landscape, dominated by a large set of waveforms that produced minimal neural effects and a small subset that elicited selective, component-specific effects that varied across individuals. These findings demonstrate that EVS–EEG interactions are sparse, waveform-dependent, and subject-specific, and highlight the utility of GC-based modeling for organizing heterogeneous stimulation responses and informing future data-driven and personalized neuromodulation strategies.**

Keywords— Electroencephalography (EEG), Electrical vestibular stimulation (EVS), Granger Causality (GC), Parkinson's Disease (PD)

I. Introduction

Electrical Vestibular Stimulation (EVS) is a non-invasive brain stimulation (NIBS) technique in which weak electrical currents are delivered through electrodes placed over the bilateral mastoid processes, modulating activity within the vestibular apparatus and ultimately downstream associated cortical networks [1]. EVS is safe, accessible, and relatively low-cost, and has been shown to influence sensorimotor and balance-related processes, across healthy and clinical populations [2]. In Parkinson's disease (PD), EVS has been reported to improve gait, tremor, bradykinesia, and motor variability, suggesting its potential as an adjunct therapy for motor rehabilitation [3], [4]. Although EVS is noninvasive and therefore allows substantial flexibility in the design of stimulation waveforms, most studies continue to rely on a narrow set of standardized patterns, primarily direct current (DC), simple sinusoidal stimulation, or stochastic (noisy) patterns. This continued reliance on a limited set of waveforms is not driven by established efficacy, but rather by the absence of principled frameworks for EVS parameter selection. As emphasized in prior work, the lack of systematic approaches for evaluating waveform-dependent neural effects has constrained exploration of the EVS parameter space, underscoring the need for data-driven methods to assess and optimize stimulation for reliable neural and clinical outcomes [5].

To evaluate the neural effects of EVS, electroencephalography (EEG) has been used to quantify changes in brain activity. To date, EVS-induced neural effects have primarily been characterized using metrics such as spectral power, event-related potentials (ERPs), event-related desynchronization/synchronization (ERD/ERS), or functional connectivity [6]-[8]. These approaches largely rely on repeated presentations of a single stimulation protocol and are therefore well-suited for identifying averaged effects of a given stimulus. However, understanding how neural responses vary across different EVS waveforms is essential for determining how

This work was partially supported by the John Nicol chair in Parkinson's research (MJM), by the Maud Menten Research Accelerator award , NSERC Create (MK), and NSERC(AL)

stimulation is reflected in brain activity and for identifying candidate stimuli that warrant further evaluation. Capturing waveform-dependent neural effects thus calls for a framework that explicitly models the relationship between the stimulation signal and neural activity as coupled time series. Granger Causality (GC) provides such a framework by testing whether past values of one signal improve the prediction of another beyond what is explained by the target signal's own history, typically using autoregressive (AR) time-series models [9]. GC measures have been widely used in neuroscience to characterize directed interactions among neural signals in fMRI, EEG, EMG, and intracranial recordings; however, their application has primarily focused on interactions between neural signals themselves [10]– [12]. Although some studies have applied GC-based frameworks to probe stimulus–response relationships, the effects of external stimulation on neural activity remain relatively underexplored [13].

In this study, we present a GC–based stimulus–response framework to systematically characterize waveform-dependent neural effects of EVS measured with EEG. EEG was recorded from healthy controls and individuals with PD during exposure to a diverse set of 304 distinct EVS waveforms. Directed interactions between each stimulation waveform and independent EEG components were quantified using GC, and stimulation waveforms were grouped based on similarities in their GC-based neural response patterns. This analysis revealed substantial heterogeneity across waveforms, with a large subset consistently eliciting minimal neural effects across participants, while waveforms associated with stronger neural responses tended to exhibit greater subject specificity. The remainder of this paper describes the experimental design and data acquisition, the GC-based analysis and clustering methodology, the resulting waveform-dependent response patterns, and their implications for systematic and personalized EVS waveform evaluation.

II. Methodology

A. Experimental Design and Data Acquisition

EEG data were collected from ten participants, including five individuals with PD and five healthy controls. During recording, participants passively viewed neutral images to maintain engagement. Each participant completed a single experimental session consisting of 304 trials, including one sham condition and 303 unique EVS waveforms. The stimulus set spanned a broad range of waveform types and frequency characteristics, including direct current (DC), pure sinusoids (0.5–200 Hz), amplitude- and frequency-modulated signals, chirp-based waveforms, multisine patterns, and binary-modulated stimuli (see the Appendix). Each trial lasted nine seconds and comprised a 2-s pre-stimulation baseline, 2-s stimulation period, and 5-s post-stimulation interval. Trials were presented consecutively without explicit cues, and participants remained unaware of stimulus transitions. EEG signals were recorded from 36 scalp electrodes positioned according to the extended 10–20 system, at a sampling rate of 1 kHz. EVS was delivered in a random order via electrodes positioned bilaterally over the mastoid processes. Stimulation intensity was individually calibrated using a perceptual thresholding procedure, and all stimuli were delivered at subthreshold levels to minimize sensory awareness and attentional confounds. Fig. 1 Illustrates the experimental setup and trial structure.

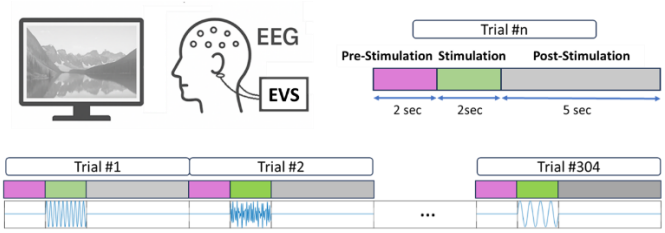

Fig. 1. Schematic overview of the experimental paradigm. Each participant underwent a single run consisting of 304 consecutive EVS trials, delivered in randomized order without inter-trial pauses. Each trial included three temporal segments: 2 seconds of pre-stimulation, 2 seconds of stimulation, and 5 seconds of post-stimulation. During stimulation, EEG signals were recorded while participants viewed neutral nature scenes on a monitor

B. Data Preprocessing

EEG was preprocessed using a multi-stage pipeline developed specifically to suppress EVS-related electrical artifacts while preserving physiological activity [14]. Raw EEG channels (36 scalp electrodes) were high-pass filtered at 0.5 Hz to remove slow drifts, 60 Hz line noise was removed (CleanLine), signals were demeaned (DC component subtracted), and data were re-referenced to the common average reference (CAR). Data were then segmented into trials using recorded stimulus-onset flags. Artifact suppression was performed on the full trial window to enable robust identification and removal of stimulation-related contamination across pre-, peri-, and post-stimulation periods. First, EVS electrical artifact was attenuated per trial using Principal Component Analysis (PCA)-based regression, where the first PC served as an estimate of the stimulation artifact and was regressed from each EEG channel. Residual stimulation- and ocular-related artifacts were then reduced using canonical correlation analysis (BSS-CCA), and components were automatically labeled using supervised SVM classifiers trained on manually labeled trials to identify EVS- and EOG-contaminated components; labeled components were removed and the signal reconstructed. Second, ICA was applied to the artifact-reduced signal and an additional SVM classifier was used to identify EMG components (along with residual EVS/EOG features), which were rejected prior to reconstruction. Finally, signals were band-stop filtered at 59–61 Hz (residual line noise) and low-pass filtered at 100 Hz. As a quality control step, trials with residual artifact signatures (assessed via the first PC of the reconstructed signal) were manually corrected by adjusting component labels. This preprocessing approach has been previously validated on the same EVS-EEG dataset and is described in detail in the companion preprocessing paper [14].

Following artifact suppression, only the 2 s EVS stimulation segments were retained for subsequent GC analysis. These stimulation segments were high-pass filtered at 1 Hz to improve component separation and z-score normalized on a per-channel basis to standardize signal variance across electrodes.

C. Stable Independent Component Extraction

Independent Component Analysis (ICA) was used to decompose EEG into statistically independent component (IC) time series for subsequent GC analysis. To obtain a trial-invariant decomposition, stimulation segments were concatenated across trials within each participant, and a single subject-level ICA decomposition was computed. Stable components were identified using the ICASSO framework (20 runs), with stability quantified by the index I_q, and only components with $I_q > 0.95$ were retained for further analysis [15].

D. Granger Causality Analysis

GC tests whether past values of the predictor time series improve prediction of the response time-series. Pairwise, time-domain GC was computed using linear AR models, with each IC time series treated as the response signal and the corresponding EVS waveform as the predictor. For each IC–waveform pair, the unrestricted AR model was defined as:

$$Y(t) = \sum_{i=1}^{p} a_k Y(t-k) + \sum_{i=1}^{p} b_k X(t-k) + \epsilon(t) \quad (1)$$

where $Y(t)$ denotes IC time series, $X(t)$ the EVS waveform, p the model order (lag), a_k and b_k the AR coefficients, and $\varepsilon(t)$ the residual error term. The restricted model excluded the stimulation terms:

$$Y(t) = \sum_{i=1}^{p} a_k Y(t-k) + \epsilon(t) \quad (2)$$

GC strength is defined by an F-statistic comparing the residual variances of the restricted and unrestricted models. Model order p was selected using the Akaike Information Criterion (AIC), evaluated up to a maximum lag of 140 ms [16]. For each participant, this procedure yielded a GC matrix of size $304 \times N$, where N is the number of stable ICs retained for analysis.

E. K-means Clustering of GC-based Response Profiles

K-means clustering was applied to the GC matrices to group EVS waveforms based on similarity in their IC-wise GC profiles. For each participant, each EVS waveform corresponded to a single row of the GC matrix (size $1 \times N$), containing the GC F-statistics across stable ICs. These row vectors served as feature representations of waveform-specific cortical responses. Prior to clustering, GC values were z-score normalized across ICs to ensure equal weighting of features. The number of clusters was determined primarily by visual inspection of elbow plots of the within-cluster sum of squares (WSS), which showed a consistent inflection around k=4 across participants. This choice was further supported by quantitative evaluation of both WSS and average silhouette scores for k = 2 to 8.

All analyses, including ICA, Granger causality computation, and clustering, were implemented in MATLAB.

III. Results

A. Granger Causality Analysis

1) Stable Independent Components: ICASSO identified between 21 and 27 stable ICs (N) in healthy controls (mean ± SD: 23.4 ± 2.06) and between 15 and 27 components in participants with PD (mean ± SD: 22.0 ± 4.82). While the number of stable components exhibited greater inter-subject variability in the PD group, the overall range and mean values were comparable to those observed in healthy controls, supporting the reliability of the ICA decomposition across groups for subsequent GC analysis.

2) Model Order and Time Delays: Model orders selected by AIC yielded a range of effective times for both HC and PD groups (Fig. 2). Given the diversity of the 304 stimulation waveforms, delays were distributed over a wide temporal range in both groups, showing substantial overlap (Fig. 2A). In HCs, delays were centred at 63.52 ± 29.49 ms, whereas PD participants showed a higher mean delay of 69.51 ± 32.02 ms (Fig. 2B). A linear mixed-effects model (Delay ~ Group + (1 | Waveform)) confirmed a significant group difference, with PD exhibiting longer delays (β = 6.74 ms, $p < 0.001$; see Fig. 2B).

3) Granger Causality F-values: Fig. 3 shows representative GC F-statistics for a single subject (HC), visualized as a GC matrix capturing directed interactions between the 304 EVS waveforms and stable ICs. In this representation rows correspond to individual stimulation waveforms and columns to ICs. GC strength varies across both dimensions, revealing a non-uniform, waveform- and component-dependent pattern of directed interactions.

B. Clustering of EVS Waveforms based on GC Profiles

K-means clustering ($k = 4$) was applied to waveform-wise GC profiles, represented as row vectors of standardized F-statistics across ICs, to group EVS waveforms based on their IC-specific directed interaction patterns. Across a range of cluster numbers (k = 2–8), clustering yielded a consistent structural organization, characterized by one dominant cluster with uniformly low GC values and multiple smaller clusters exhibiting elevated GC F-statistics confined to subsets of ICs.

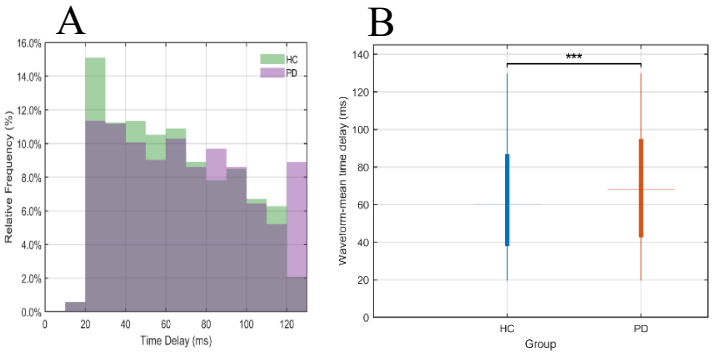

Fig. 2. Time delays between EVS waveforms and EEG responses. (A) Histograms of AIC-selected delays (10 ms bins) for HC and PD groups. (B) Group-level boxplots *** denotes significant group difference ($p < 0.001$, linear mixed-effects model with random intercept for waveform).

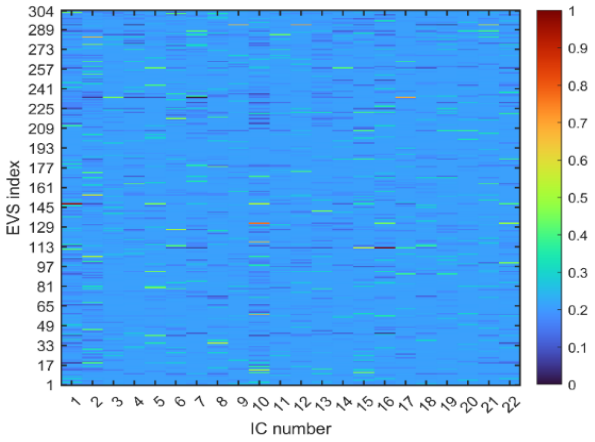

Fig. 3. Heatmap of normalized GC F-values between EVS waveforms and ICs for a representative subject.

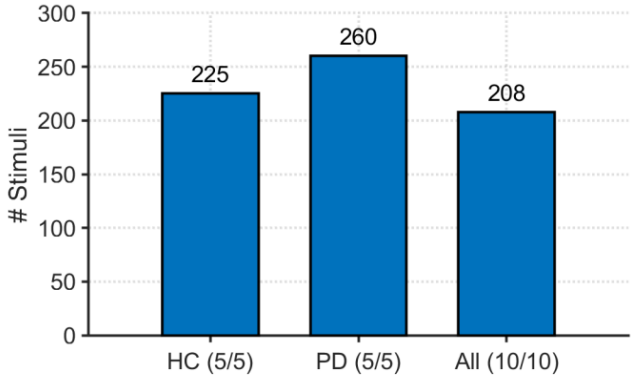

Fig. 5. Number of EVS waveforms consistently assigned to the low-GC cluster across all subjects including for healthy controls (HC, m = 5), Parkinson's disease participants (PD, m = 5), and all participants combined (HC+PD, m = 10).

Fig. 4A illustrates the distribution of the 304 EVS waveforms across clusters for the representative HC subject, revealing a highly imbalanced structure in which the majority of waveforms (n = 277) were assigned to a single dominant cluster, while the remaining waveforms were distributed across three smaller clusters (n = 5, 7, and 15). Importantly, this imbalanced clustering structure was consistently observed across all subjects, with one dominant low-GC cluster and three substantially smaller clusters. Fig. 4B shows the corresponding cluster centroids, defined as the mean standardized GC F-statistics across ICs for each cluster. The dominant cluster exhibited uniformly low GC values across components, whereas the smaller clusters showed IC-specific elevations in GC, indicating waveform- and component-dependent GC structure. A similar centroid structure was observed across subjects. Fig. 4C shows IC11 and IC19 from cluster 3 exhibiting elevated GC values.

C. *Cross-Subject Consistency of Low-GC EVS Waveforms*

A substantial subset of EVS waveforms were consistently classified within the low-GC cluster across participants. As shown in Fig. 5, 225 of the 304 waveforms were assigned to the low-GC cluster in all HC participants (5/5), while 260 waveforms showed the same consistency across all PD participants (5/5). When both groups were considered jointly, 208 waveforms were consistently classified within the low-GC cluster across all subjects (10/10). These findings demonstrate that the majority of EVS waveforms exhibit reproducibly low GC values across individuals, with a larger proportion of such waveforms observed in the PD group compared to HCs.

D. *Cross-Subject Consistency of High-GC EVS Waveforms*

In contrast to the low-GC cluster, EVS waveforms assigned to the high-GC clusters showed limited cross-subject consistency (Fig. 6). In HCs ($m = 5$), the majority of high-GC waveforms were observed in only a single participant ($n = 50$), with progressively fewer waveforms shared by two ($n = 21$), three ($n = 5$), or four ($n = 3$) participants, and none shared across all five HCs (Fig. 6). A similar pattern was observed in the PD group (m = 5), where most high-GC waveforms appeared in only one participant ($n = 36$), with limited overlap across two ($n = 5$) or three ($n = 3$) participants and no waveforms shared by four or five individuals. When

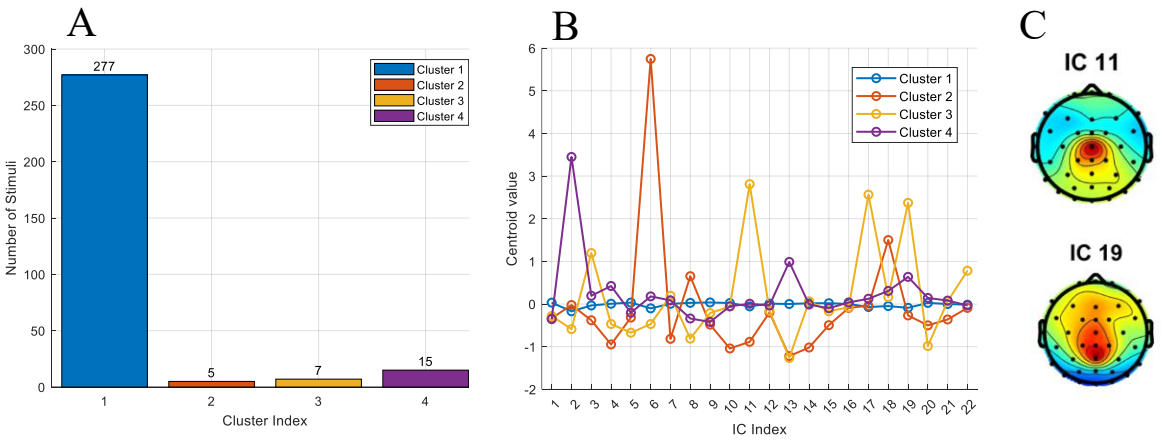

Fig. 4. Clustering of EVS stimuli based on GC features for a representative subject. (A) Distribution of stimuli across four clusters. Numbers above bars indicate the number of stimuli per cluster. (B) Cluster centroids across ICs. (C) Example ICs with elevated F-values from cluster 3.

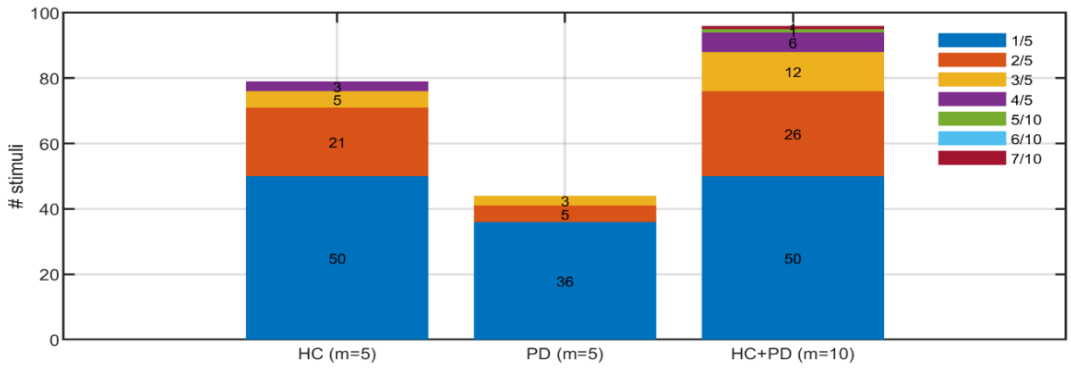

Fig. 6. Cross-subject consistency of EVS waveforms assigned to high-GC clusters. Stacked bar plots show the number of EVS waveforms classified within high-GC clusters in exactly k/m subjects for HCs (HC, m = 5), PD participants (PD, m = 5), and all participants combined (HC+PD, m = 10). Colors indicate the number of subjects (k) in which a given waveform was identified as high-GC.

considering all participants jointly (HC+PD; $m = 10$), high-GC waveforms again showed minimal cross-subject consistency: most were observed in a single subject ($n = 50$), with steadily decreasing overlap across larger subsets of participants, and only two waveforms shared by five or more individuals ($\geq 5/10$). EVS waveforms most frequently ranked among high-GC stimuli within each group are summarized in Table I. One waveform that emerged consistently across both groups was the chirp amplitude-modulated (AM) signal with a 75 Hz carrier and 4–8 Hz chirp envelope. Although the carrier frequency was 75 Hz, the modulation envelope varied at theta-range timescales (4–8 Hz). This is noteworthy because theta-band activity has been strongly linked to vestibular processing, hippocampal-cortical communication, and sensorimotor integration, and prior vestibular stimulation studies have demonstrated modulation of theta rhythms [18,19]. The prominence of this waveform may therefore reflect preferential sensitivity of vestibular–cortical networks to low-frequency temporal modulation patterns. However, these interpretations remain speculative, as the present study was not designed to test specific physiological mechanisms underlying waveform selectivity.

IV. Discussions and Conclusion

In this study, we applied a GC-based framework to systematically characterize waveform-dependent influences of EVS on EEG activity in HCs and individuals with PD.

TABLE I. Group-specific EVS waveforms most frequently ranked among high-GC stimuli

HC (4 of 5 participants)	PD (3 of 5 participants)	Shared (2 of 5 HC and 2 of 5 PD)
BN-modulated 4-8 Hz	Chirp High 2	Sinusoidal (AC) 1.40 Hz
chirp AM Carrier: 100 Hz, chirp: 12-30 Hz	Multisine MVS-L[17]	
chirp AM Carrier: 75 Hz, chirp: 4-8 Hz	chirp AM Carrier: 75 Hz, chirp: 4-8 Hz	chirp AM Carrier: 75 Hz, chirp: 4-8 Hz

By quantifying directed interactions between stimulation waveforms and independent EEG components, and organizing waveforms based on their causal influence profiles, we identified a highly structured organization of the EVS parameter space. This organization was dominated by a large set of minimally effective waveforms and a small number of clusters exhibiting selective neural effects. These effects were sparse and varied across individuals, indicating that EVS–EEG interactions are strongly stimulus- and subject-dependent rather than uniformly driven by stimulation. In addition, GC-derived delay estimates revealed significant differences in temporal organization, with longer delays in the PD group ($\beta = 6.74$ ms, $p < 0.001$), consistent with altered network dynamics in PD. This slowing of causal influence may reflect disrupted cortico-basal ganglia or vestibular-cortical processing, although further work is needed to link these temporal changes to clinical symptoms

The coexistence of a dominant minimally effective group of stimuli that overlaps across subjects alongside a small number of selective, largely subject-specific response patterns has important implications for how EVS is typically evaluated. Standard approaches based on repeated presentation of a single or small set of canonical waveforms implicitly assume that the applied stimulus is effective and representative. The present findings, consistent with prior observations of variability in EVS outcomes, challenge this assumption by demonstrating that neural responses are strongly parameter-specific and that most waveforms produce negligible effects across participants. In contrast, effective responses occupy a narrow and discontinuous subset of the stimulation space and differ across individuals. Although the present study does not establish behavioral or clinical relevance, it provides a principled, data-driven framework for identifying candidate stimulation patterns that warrant further evaluation. In this context, AR modeling approaches such as Granger causality offer a systematic means of organizing stimulation–response relationships and are complementary to ongoing efforts aimed at developing adaptive neuromodulation strategies.

A key consideration is whether the observed GC patterns could reflect direct electrical contamination of the EEG by the

EVS signal rather than stimulus-driven neural interactions. Several features of the results argue against a simple leakage explanation. Across all subjects, clustering consistently revealed one dominant minimally effective cluster characterized by near-zero GC values across ICs, indicating that the majority of waveforms produced negligible coupling to EEG activity. If the results were dominated by nonspecific electrical leakage, more widespread effects across waveforms would be expected under a fixed stimulation and recording configuration. Instead, elevated GC effects were confined to a small number of smaller clusters and were expressed in only a limited subset of components, reflecting sparse and selective responses rather than widespread coupling. Importantly, while the overall clustering structure was preserved across subjects, the specific waveforms and components associated with higher-effect clusters varied between individuals suggesting subject-specific sensitivities rather than a single stable leakage pattern. Finally, GC effects peaked at nonzero, structured delays rather than near-zero lags, a pattern that is inconsistent with instantaneous electrical contamination and more consistent with temporally mediated neural interactions. Together, these observations suggest that the GC patterns reflect structured, stimulus-dependent interactions that cannot be readily explained by nonspecific electrical artifact alone

The scope of the present study should be considered when interpreting the findings. The analysis was conducted in a relatively small cohort (five HCs and five individuals with PD), reflecting the study's primary goal of characterizing waveform-dependent neural interactions and identifying structure in stimulation–response relationships rather than drawing clinical or behavioral conclusions. Within this scope, the reproducibility of the overall clustering structure across participants supports the presence of stimulus-dependent neural effects. An important next step will be to establish the behavioral and clinical relevance of these neural responses. While certain waveforms elicited reproducible EEG effects, their relationship to functional or therapeutic outcomes remains unknown. Future work should therefore integrate behavioral and clinical measures and explore individualized stimulation strategies to link neural responsiveness to functional improvement.

ACKNOWLEDGMENT

The authors would like to acknowledge Mahdi Babaei for assistance with data preprocessing. We also thank Martin Keung, Hanaa Diab, Varsha Sreenivasan, and Juana Ayala for their contributions to the experimental setup, participant recruitment, and protocol execution.

REFERENCES

[1] J. Dlugaiczyk, K. D. Gensberger, and H. Straka, "Galvanic vestibular stimulation: from basic concepts to clinical applications," J. Neurophysiol., vol. 121, no. 6, pp. 2237–2255, 2019.

[2] A. P. B. de Ávila Pires, T. R. Silva, M. S. Torres, M. L. Diniz, M. C. Tavares, and D. U. Gonçalves, "Galvanic vestibular stimulation and its applications: a systematic review," Braz. J. Otorhinolaryngol., vol. 88, pp. S202–S211, 2022.

[3] S. Lee, A. Liu, and M. J. McKeown, "Current perspectives on galvanic vestibular stimulation in the treatment of Parkinson's disease," Expert Rev. Neurother., vol. 21, no. 4, pp. 405–418, 2021.

[4] M. Khoshnam, D. M. C. Häner, E. Kuatsjah, X. Zhang, and C. Menon, "Effects of galvanic vestibular stimulation on upper and lower extremities motor symptoms in Parkinson's disease," Front. Neurosci., vol. 12, Art. no. 633, 2018.

[5] Y. Valter, L. Vataksi, A. R. Allred, J. R. Hebert, T. T. Brunyé, T. K. Clark, J. Serrador, and A. Datta, "A review of parameter settings for galvanic vestibular stimulation in clinical applications," Front. Hum. Neurosci., vol. 19, Art. no. 1518727, 2025.

[6] A. Kazemi, M. S. Mirian, S. Lee, M. J. McKeown , "Galvanic vestibular stimulation effects on EEG biomarkers of motor vigor in Parkinson's disease," Front. Neurol., vol. 12, Art. no. 759149, 2021.

[7] L.-W. Ko, et al., "Noisy galvanic vestibular stimulation (stochastic resonance) changes electroencephalography activities and postural control in patients with bilateral vestibular hypofunction," Brain Sci., vol. 10, no. 10, Art. no. 740, 2020.

[8] S. J. Duncan, K. Marques, J. Fawkes, L. J. Smith, and D. T. Wilkinson, "Galvanic vestibular stimulation modulates EEG markers of voluntary movement in Parkinson's disease," Neuroscience, vol. 555, pp. 178–183, 2024.

[9] C. W. J. Granger, "Investigating causal relations by econometric models and cross-spectral methods," Econometrica, vol. 37, no. 3, pp. 424–438, 1969.

[10] R. Coben and I. Mohammad-Rezazadeh, "Neural connectivity in epilepsy as measured by Granger causality," Front. Hum. Neurosci., vol. 9, Art. no. 194, 2015.

[11] A. K. Seth, A. B. Barrett, and L. Barnett, "Granger causality analysis in neuroscience and neuroimaging," J. Neurosci., vol. 35, no. 8, pp. 3293–3297, 2015.

[12] A. Roebroeck, E. Formisano, and R. Goebel, "Mapping directed influence over the brain using Granger causality and fMRI," NeuroImage, vol. 25, no. 1, pp. 230–242, 2005.

[13] G. Acharya, K. A. Davis, and E. Nozari, "Predictive modeling of evoked intracranial EEG response to medial temporal lobe stimulation in patients with epilepsy," *Commun. Biol.*, vol. 7, no. 1, Art. no. 1210, 2024.

[14] M. Babaei, S. H. Sardouie, M. Keung, V. Sreenivasan, H. Diab, M. S. Mirian, and M. J. McKeown, "Semi-automatic multi-stage artifact removal in EEG during subthreshold GVS: A machine learning approach for neuromodulation studies," in *Proc. 32nd Nat. 10th Int. Iranian Conf. Biomed. Eng. (ICBME)*, Nov. 2025, pp. 1177–1183.

[15] J. Himberg and A. Hyvärinen, "ICASSO: software for investigating the reliability of ICA estimates by clustering and visualization," in Proc. Int. Workshop Neural Networks for Signal Processing (NNSP), Toulouse, France, pp. 259–268, 2003.

[16] H. Akaike, "A new look at the statistical model identification," *IEEE Trans. Autom. Control*, vol. 19, no. 6, pp. 716–723, 1974.

[17] P. A. Forbes, *et al.*, "Electrical vestibular stimuli to enhance vestibulo-motor output and improve subject comfort," *PLoS One*, vol. 9, no. 1, Art. no. e84385, 2014.

[18] P. Aitken, Y. Zheng, and P. F. Smith, "The modulation of hippocampal theta rhythm by the vestibular system," *J. Neurophysiol.*, vol. 119, no. 2, pp. 548–562, 2018

[19] S. Karakaş, "A review of theta oscillation and its functional correlates," *Int. J. Psychophysiol.*, vol. 157, pp. 82–99, 2020.

Appendix

TABLE II. LIST OF ALL STIMULI

Category	Stimuli Description	Stimulus IDs
Baseline & DC	Sham, Pink Noise, DC +1, DC -1	1–4
Chirp Signals	Delta, Theta, Alpha, Beta, Gamma, High 1–3	5–12
Sinusoidal (AC)	0.5 Hz to 200 Hz in ~1 Hz increments	13–213
Multisine	Theta, Alpha, Beta, Gamma, High 1–3, MVS variants	214–223
AM	Carrier: 75/100/125 Hz; Envelope: 9/11/16/25 Hz	224–247
Chirp AM	Carrier: 75/100/125 Hz; Chirp: Delta–Gamma	248–275
FM Signals	Carrier: 75/100/125 Hz; Modulation: 9/11/16/25 Hz	276–287
PAC Signals	Phase-Amplitude Coupling: combinations of Delta–Gamma bands	288–297
BN-Modulated Signals	Band-limited noise modulated: Delta, Theta, Alpha, Beta, Gamma, High 1–2	298–304